

Millimeter wave imaging system for the detection of non-metallic objects

Todd W. Du Bosq^{a,b}, Jose M. Lopez-Alonso^a, Glenn D. Boreman^{a,b}, David Muh^c,
Jeffrey Grantham^c, Daniel Dillery^c

^aCollege of Optics and Photonics, CREOL, University of Central Florida,

^bDepartment of Physics, University of Central Florida,
4000 Central Florida Blvd., Orlando, FL USA 32816-2700

^cNorthrop Grumman Corporation
Integrated Systems Sector Airborne Ground Surveillance & Battle Management Systems
P.O. Box 9650 M/S K11-219, Melbourne, FL 32902-9650

ABSTRACT

With over 110 million landmines buried throughout the world, the ability to detect and identify objects beneath the soil is crucial. The increased use of plastic landmines requires the detection technology to be able to locate both metallic and non-metallic targets. A novel active mmW scanning imaging system was developed for this purpose. It is a hyperspectral system that collects images at different mmW frequencies from 90-140 GHz using a vector network analyzer collecting backscattering mmW radiation from the buried sample. A multivariate statistical method, Principal Components Analysis, is applied to extract useful information from these images. This method is applied to images of different objects and experimental conditions.

Keywords: landmines, plastic, millimeter wave, unexploded ordnance, principal component analysis

1. INTRODUCTION

Landmines inflict high costs on civilian populations many years after the military conflicts that prompted their deployment have ceased. The United Nations estimates that over 110 million active mines lie hidden beneath the ground of sixty-eight countries, killing or maiming 2000 people per month. Accidents occur on a rate of one for every 1000 to 2000 mines destroyed.¹ The threat to civilians remains and hinders economic and social recovery.

Anti-personnel mines are usually buried just beneath the surface to a depth of about 3 cm, whereas anti-tank mines are buried as deep as 40 cm. The landmines can be any shape and be made of many different materials including metal, plastic, rubber, or wood. There are a number of detection technologies applied for the remediation of minefields,² such as inductance coils³ (metal detectors), magnetometers, ground-penetrating radar³, infrared imaging⁴, and explosives vapor sensors.² Metallic mines can be detected using many of the methods mentioned above. However, the increased use of plastic mines has made detection difficult. A passive mmW landmine detection system has been demonstrated before,⁵ but depends on the effective sky temperature. An active mmW system⁶ is potentially attractive in that, in an imaging mode, it can achieve good discrimination between anti-personnel mines that are primarily non-metallic, and the small metallic debris (shrapnel, cartridge cases, etc.) typical of minefield conditions. Because of the shape and size discrimination inherent in an imaging system, the tradeoff between false alarm rate and miss rate is favorable for mmW wavelengths.⁵ Ability to detect and image buried objects will depend on soil transmission and scattering. Soils with particle sizes larger than the wavelength have low transmittance due to scattering.⁷ Dry quartz sand has high transmission in the mmW range due to its fairly uniform particle size, which is smaller than the wavelength of light.⁷

A hyperspectral 90-140 GHz mmW imaging system used to locate and identify landmines and other objects buried beneath sand of various depths and conditions is demonstrated. The information provided by the hyperspectral images is analyzed through a Principal Component Analysis (PCA) method. With this signal processing, valuable information is condensed into single images and the buried objects can be located and identified. The PCA method has been used

before as a landmine detection signal processing technique in other wavelength regions improving the detection and classification rates while lowering the false-alarm rate.⁸⁻¹⁰ We present the experimental set up for the 90-140 GHz mmW imaging system, the signal processing method used, and imaging results of the buried objects.

2. EXPERIMENTAL METHODS

An imaging system was developed for the mmW range using an Anritsu vector network analyzer (VNA) operating from 90-140 GHz. The VNA modules, equipped with 16 degree horn antennas, were mounted on a vertically oriented optical table, shown in fig. 1. The mmW radiation was focused using a high density polyethylene (HDPE) lens onto the sample and then reflected back through another HDPE lens into the VNA receiver. Two motorized translation stages, with 200 mm maximum travel distance and 50 mm/s maximum velocity were mounted perpendicular to each other. The sample was attached to the stages using a long aluminum arm with the inset removed preventing the sample from being held over the highly reflective metal stages.

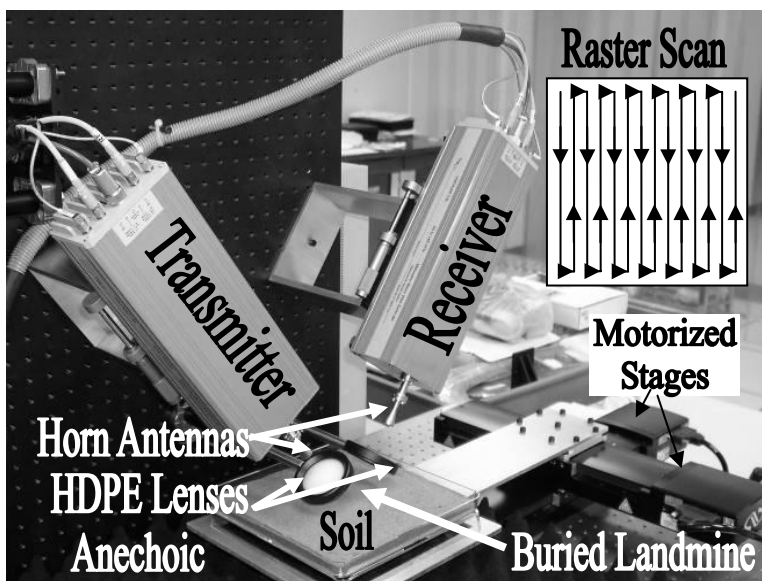


Fig. 1. Photograph of the active hyperspectral mmW imaging system. (Inset) Schematic of the path for taking a raster scan image. The radiation coming from the transmitter, 90-140 GHz, is focused onto the sample using the HDPE lens and scattering radiation from the object is collected and focused on the receiver at each pixel of the raster scan.

The landmine was placed in a 20.3 cm x 20.3 cm x 9.5 cm container surrounded by soil. This container allows the landmine to be buried up to 5 cm deep and be placed anywhere within the 412 cm². A broadband convoluted foam millimeter wave absorber, ECCOSORB CV, was placed under the sample to eliminate back reflections from the optical table. A program was written in LABVIEW to capture a raster scan image (fig. 1 inset), containing 29 lines, of the landmine under the soil. At each position of the scan, the VNA measured the reflection from the landmine, from 90-140 GHz in 1 GHz steps. The resulting data set is converted into a set of images (one for each mmW frequency used) by a MATLAB software program. In our case, the total number of frequencies is 51. The size of the images depends on the number of points taken in each scan and the distance between them. These sizes can be changed with the LABVIEW program.

The objects imaged beneath the soil were two landmines, minefield debris, and 11 pucks of various materials. The two landmines were the TS-50 (fig. 2 top left) and the M14 (fig. 2 bottom left). They are typically scatter laid by a helicopter or buried to a depth of 30 mm.¹¹ The TS-50 is a circular plastic bodied mine with strengthening ribs. The TS-50 has a height of 45 mm, a diameter of 90 mm, and weighs 186 g. It contains a round metallic pressure plate on top of the mine. The TS-50 contains 50 g of T4 explosive and is waterproof and non-buoyant.¹¹ The TS-50 cannot be located using metal detectors under most field conditions and are highly resistant to blast overpressure clearance methods. The M14 landmine is a cylindrical bodied plastic mine with very low metal content. The M14 has a height of 40 mm, a diameter of

56 mm, and weighs 90 g. The M14 contains 29 g of Tetryl explosive.¹¹ The M14 is very difficult to locate using metal detectors under most field conditions and can be defeated using blast overpressure methods. The minefield debris consisted of a 20 mm OICW practice round, a 20 mm round from WWII, a 7.62 mm cartridge case, a 5.56 mm rose crimp cartridge case, a 5.56 mm standard cartridge case, and a fuse lighter with a metal key ring (fig. 2 right).

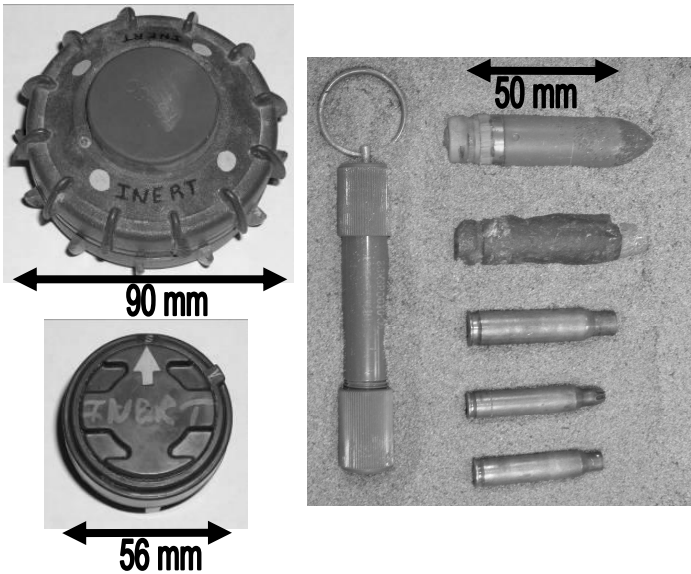


Fig. 2. Photographs of the TS-50 landmine (top left), the M14 landmine (bottom left), and minefield debris (right) including from top down a 20 mm OICW practice round, a 20 mm WWII round, a 7.62 mm cartridge case, a 5.56 mm rose crimp cartridge case, a 5.56 mm standard cartridge case, and on left a fuse lighter with a metal key ring.

The 11 pucks were 5 cm in diameter and made from Aluminum, Polystyrene, Plexiglas, HDPE, PVC, Teflon, Phenolic, Lucite, Particleboard, Plywood, and Pinewood of various thickness. The soil sample was quartz sand locally sourced at the University of Central Florida in Orlando, FL. The soil was dry and maintained in a laboratory environment at about 40% humidity.

3. SIGNAL PROCESSING

The initial data set is a collection of N images, each one corresponding to a mmW frequency. Fig. 3 shows six of the 51 individual images, representing a different frequency, taken during a single scan. The information contained in each image about the object (TS-50 landmine, fig. 2 top left) is slightly different and you cannot distinguish whether the object is a landmine, rock, aluminum can, or some other minefield debris. The information about the structure of the object is not concentrated around a single frequency but spread over the frequency spectrum. Therefore, it is necessary to employ a method that can combine the majority of the available information into a single image with a high signal to noise ratio.

For this purpose, we have used a Principal Component Analysis (PCA) method. PCA is a multivariate statistical method primary developed to deal with a large ensemble of observations of N random variables.¹² The original data set is the collection of N images, parameterized by the frequency f . The N images are each transformed to produce a mean of zero. In this framework, the N images are N random variables and the values of the pixels are “random observations”. The covariance matrix between the N images is calculated.¹³ In general, this matrix is strongly non-diagonal, which means there is a strong correlation between the images (see fig. 3).

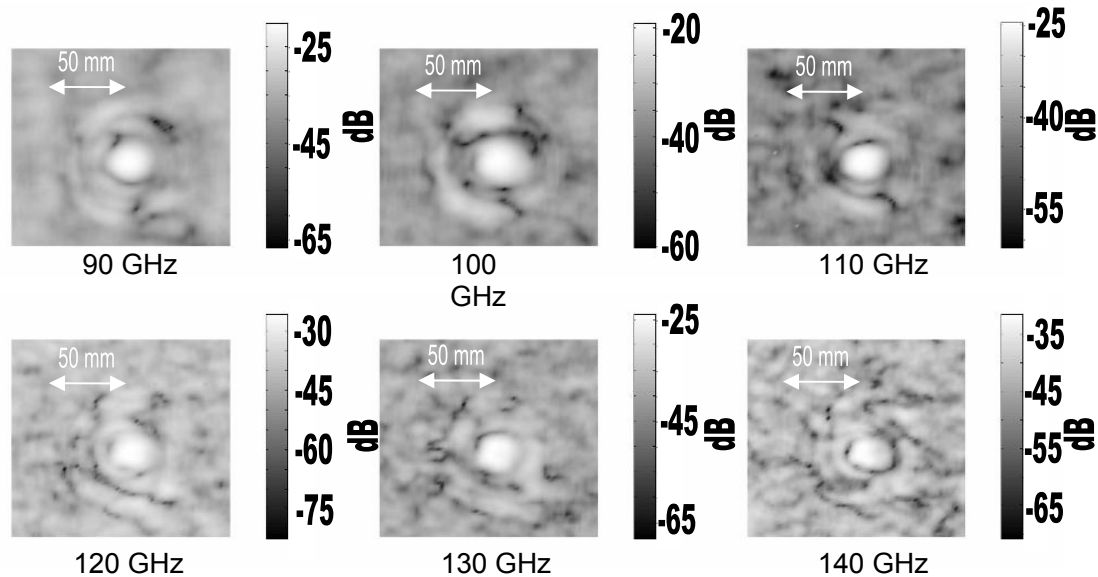


Fig. 3. Six of the 51 single-frequency reflectance images taken from 90-140 GHz in 1 GHz steps of the TS-50 landmine with a 2 mm step size, buried 15 mm deep, and with a flat soil surface.

Principal components are a new set of variables (frames) that have no correlation between them. Moreover, the original frames can be seen as a linear combination of the principal components. The coefficients of these linear combinations are obtained through the diagonalization of the frame covariance matrix, giving the eigenvalues, the eigenvectors, and the principal components. The principal components can be seen as the projections of the original zero mean images into a base produced by the eigenvectors. After the diagonalization, there is zero correlation between the principal components Y_α and they are calculated as linear combinations of the original images. But, the original images can be expressed as linear combinations of the principal components. Normally, the principal features of the data set are well represented by a few number of principal components.¹⁴ In our case, the principal features of the landmine are well represented by only one principal component (Y_1 in fig.4). This allows the main principal components to be selected and then to reconstruct the original images using only them, filtering out the higher components. This process is called rectification.¹³ A statistical analysis of the principal component decomposition enables the classification and grouping of the eigenvalues and the corresponding eigenimages into processes. When a subset of eigenvalues, along with their uncertainty, can be consecutively indistinguishable, they belong to the same process. A process is defined as a filtered set of frames generated by a subset of principal components. These processes could contain a single principal component or a high number of them. Based on previous applications of the method to different types of systems,¹⁵⁻¹⁷ different types of noise are associated with process containing a high number of principal components: they are so random that they need a high number of degrees of freedom to describe them. On the other hand, “signals” normally appear associated to processes with only one principal component or a few number of them.

We have applied the previously described method to the collection of images produced by the mmW imager. After identifying the appearing processes, an analysis over the rectified images for each process is performed. The outputs are related to physical characteristics of the sample objects. These results are described in the following sections.

4. RESULTS

4.1 TS-50 Landmine

Fig. 4 shows the results of the PCA method for the set of 51 images some of which are presented in fig. 3. A relevant principal component clearly appears and its picture resembles, with high accuracy, the shape of the object buried beneath the sand. The higher principal components are grouped together in a single process which gives useful information about

the structure and composition of the object. Fig. 5 represents the total amount of variance explained by each principal component. The first principal component only represents about 27% of the total variance.

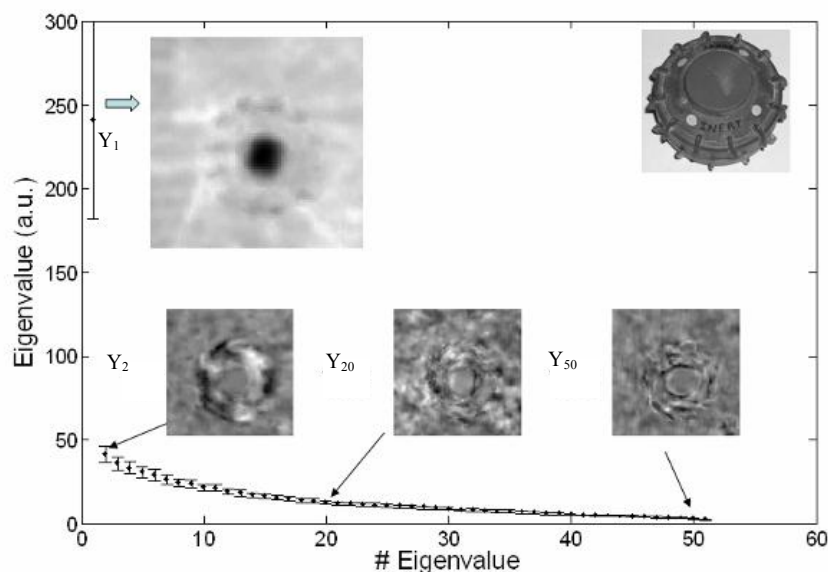


Fig. 4. Application of the PCA to a set of 51 single frequency images of the TS-50 landmine. Only one relevant principal component (Y_1) appears. Some of the higher components (Y_2 , Y_{20} , and Y_{50}) are represented.

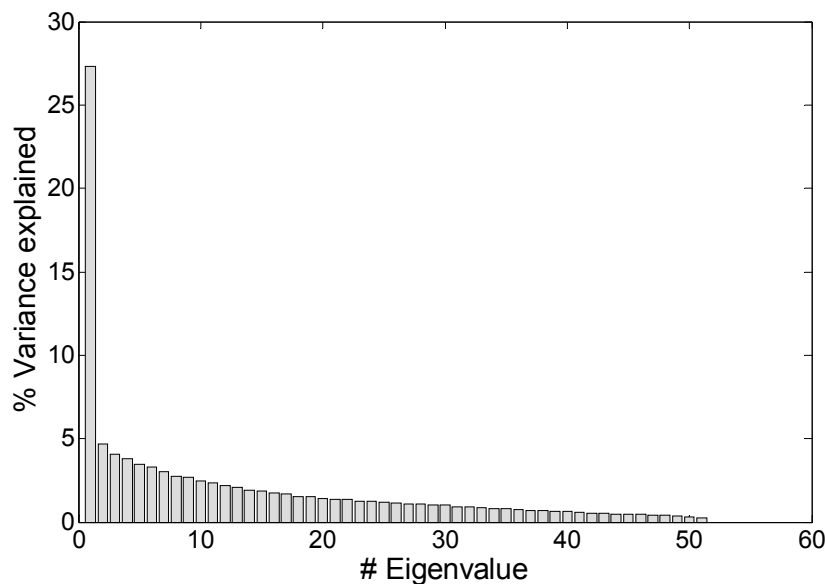


Fig. 5. Percentage of variance explained by the principal components in fig. 4.

Two different sub-data sets were constructed: the first one coming from the rectification using only the first principal component and the second from the rectification using the higher components. For each data set, the mean value and the standard deviation of each pixel is calculated and three images are constructed: the mean value (signal), the standard deviation (STD) and the ratio of them (signal to noise ratio-SNR). The results are shown in fig. 6.

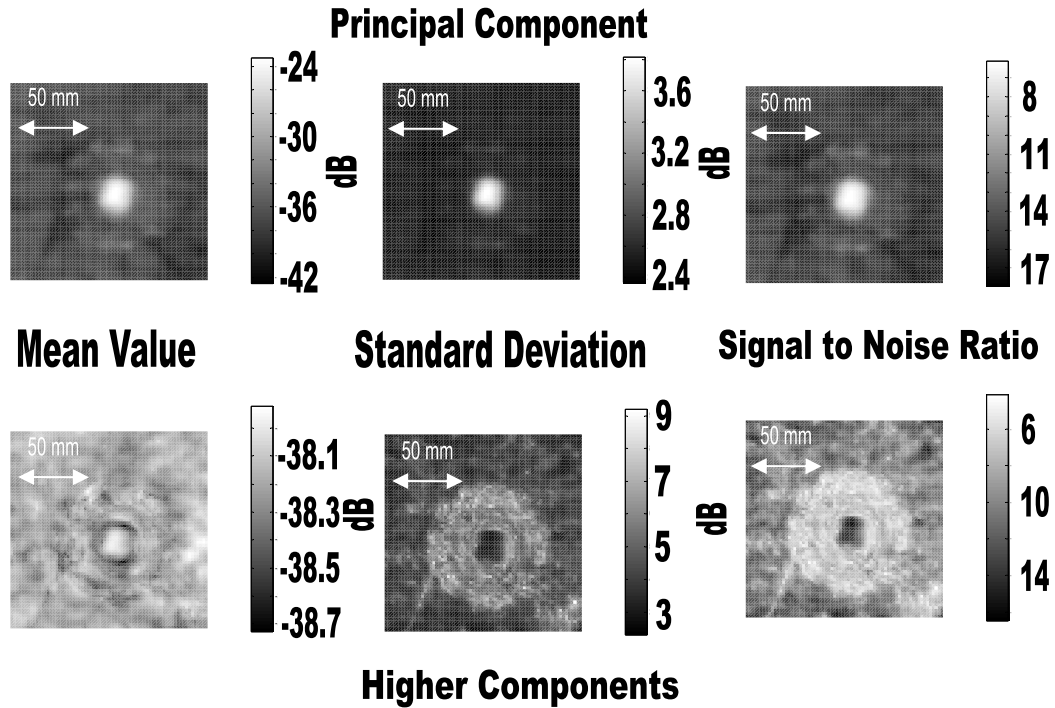


Fig. 6. Images of the mean value, standard deviation and signal to noise ratio for the rectified images of fig. 2 with the first principal component (left) and the higher components (right) of a TS-50 landmine at 2 mm step size, 15 mm deep, and with a flat soil surface.

The first principal component reconstructs the original shape of the object with high accuracy and high signal to noise ratio (typically 6 to 18). The threshold value of the signal to noise ratio for which the target is detectable half the time was determined experimentally in [18] to be between 2 to 3. The metal inside of the mine is clearly seen in the signal, meaning that the metal reflection drives it. However, reflections from the plastic body of the mine showing the structure of the strengthening ribs are seen.

We also reconstruct the data using the remaining components (higher components) and perform the same analysis as before obtaining the signal, STD, and SNR. In the reconstruction with the higher components, the signal is weaker, but the standard deviation is high. The difference in the structure and material of the background and object is responsible for this behavior. The plastic part of the object is curved and the reflection changes with the angle, while the background is random. Also, the reflection from the plastic varies at different frequencies which will be represented by the higher order components. This is the reason the STD of the higher order components is greater than the STD of the first principal component. The main difference is that while a strong signal is produced mainly by metal components of the object, the structure in the higher components is mainly driven by the structure of the plastic material.

4.2 M14 Landmine

Antipersonnel mines vary widely in size, shape, and material content depending on their intended use and burial location. The M14 landmine has a different size and shape compared with the TS-50 as well as a much smaller metal content. Images were taken for the M14 landmine with a 2 mm step size, buried 15 mm deep, and with a flat soil surface. As with the previous mine, the PCA method allows the structure and composition of the mine to be identified. The results are given in fig. 7. The unique structure of the top cap of the mine can be identified from the principal component images. The higher component images show the plastic composition of the landmine. The percentage of variance explained by the first principal component is similar to the previous case.

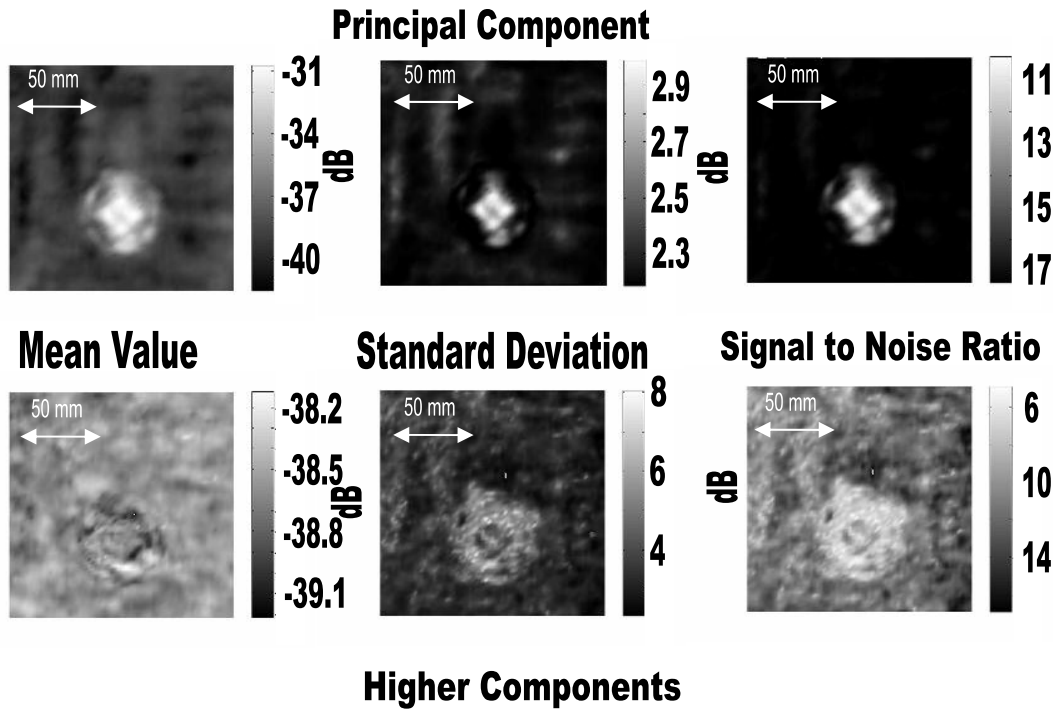


Fig. 7. Images of the mean value, standard deviation and signal to noise ratio for the rectified images of an M14 landmine with the first principal component (left) and the higher components (right) at 2 mm step size, 15 mm deep, and with a flat soil surface.

4.3 Unexploded Ordnance

Fig. 8 shows the results of the analysis for a collection of bullet cartridges and other types of minefield debris. In this case, the object is not visible in the first principal component, but in the STD of the reconstruction with the higher components. The curvature of the objects introduces deviations in the reflection coefficients. In the previous images, the metal was large and planar compared to the wavelength, which produce strong reflections. In this case the dimensions of the metal parts are small or comparable to the wavelength, producing small backscattering. The objects are curved and the reflection changes with the angle introducing a high STD. The PCA method can even distinguish between the objects with such small fluctuations allowing the minefield debris to be located and identified.

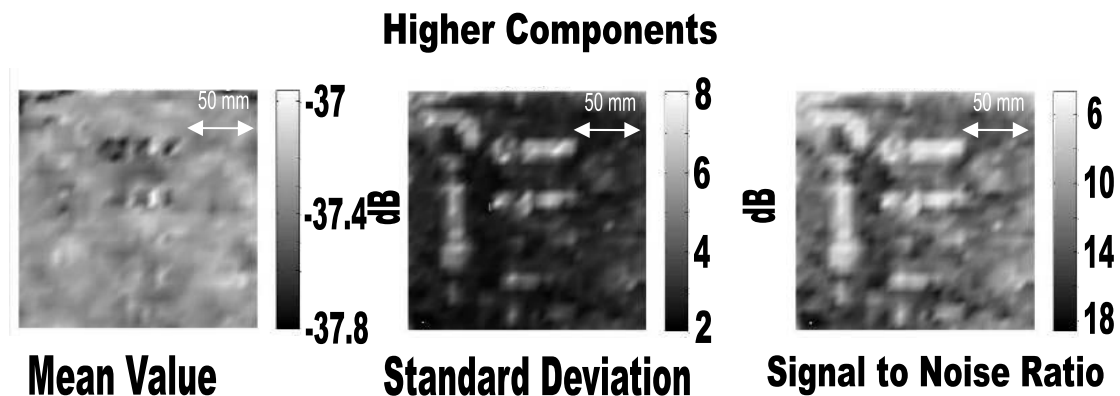


Fig. 8. Images of the mean value, standard deviation and signal to noise ratio for the rectified images of the minefield debris with the higher components at 2 mm step size, 15 mm deep, and with a flat soil surface. The principle component rectified images did not show any features of the objects.

4.4 Non-metallic materials

The results of the SNR analysis of 11 different material pucks buried 5 cm beneath the soil are shown in figs. 9 and 10. The images represent different types of non-metallic materials that can potentially be found in landmines in particular plastic and wood. The ability to locate and identify objects made of different materials beneath soil will help reduce the false alarm rate.

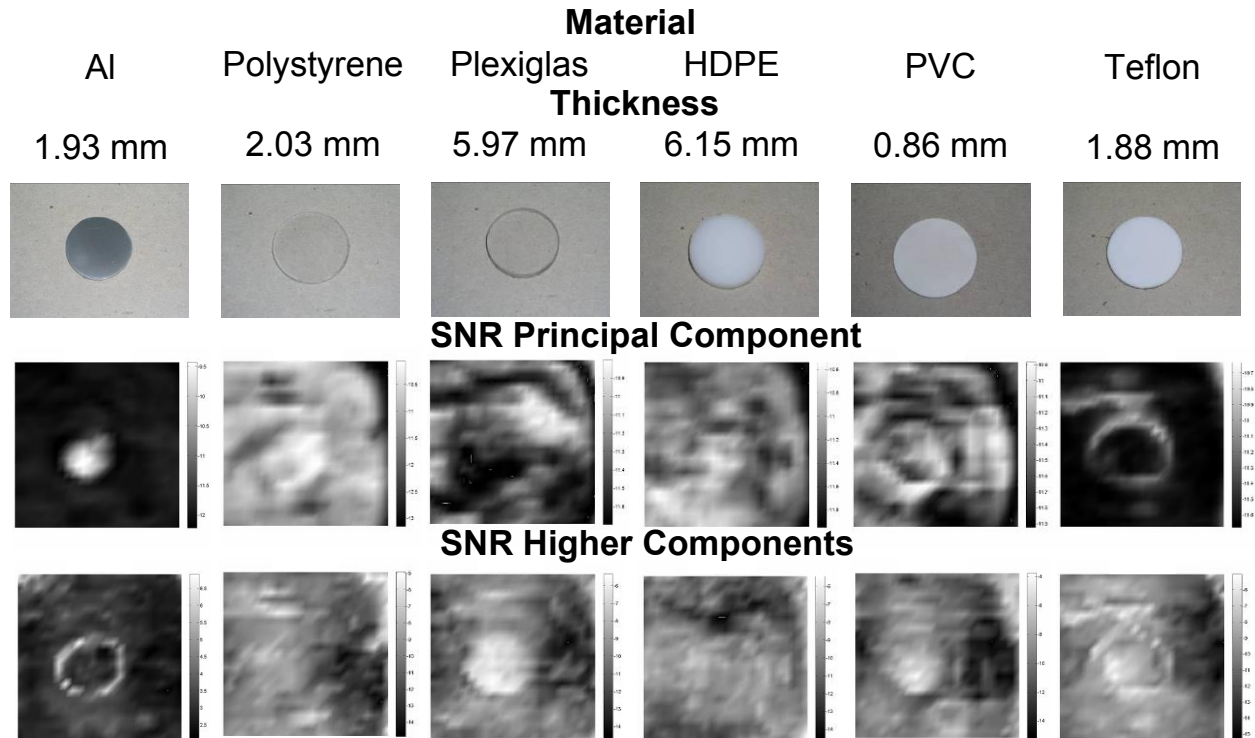


Fig. 9. Images of the SNR of the principal and higher components of 6 pucks 5 cm in diameter of various thickness made of Aluminum, Polystyrene, Plexiglas, HDPE, PVC, and Teflon buried 5 cm beneath soil, at 5 mm step size, and flat soil surface.

An aluminum puck was imaged to produce a highly reflective object for comparison with the other materials. The SNR of the principal component for the aluminum is high and the puck can be clearly seen beneath the 5 cm of soil. The reflection from the aluminum is constant over the wavelength range, except for diffraction around the edge of the puck. Therefore, the image of the SNR of the higher components for the aluminum puck only contains the outline of the puck. The reflection from the plastic and wood vary over the wavelength range allowing the puck to be clearly seen in the higher components SNR image using the PCA method. In some cases, the structure of the object can be identified in the principal component SNR. The images of the polystyrene and HDPE are not as apparent as the other plastics. Polystyrene and HDPE are highly transparent materials in the 90-140 GHz range producing small reflections under 5 cm of sand. However, a signature from the puck can still be seen. Objects made of metal, plastic, or wood can be located beneath soil. The ability to detect non-metallic objects will aid in the detection of plastic landmines.

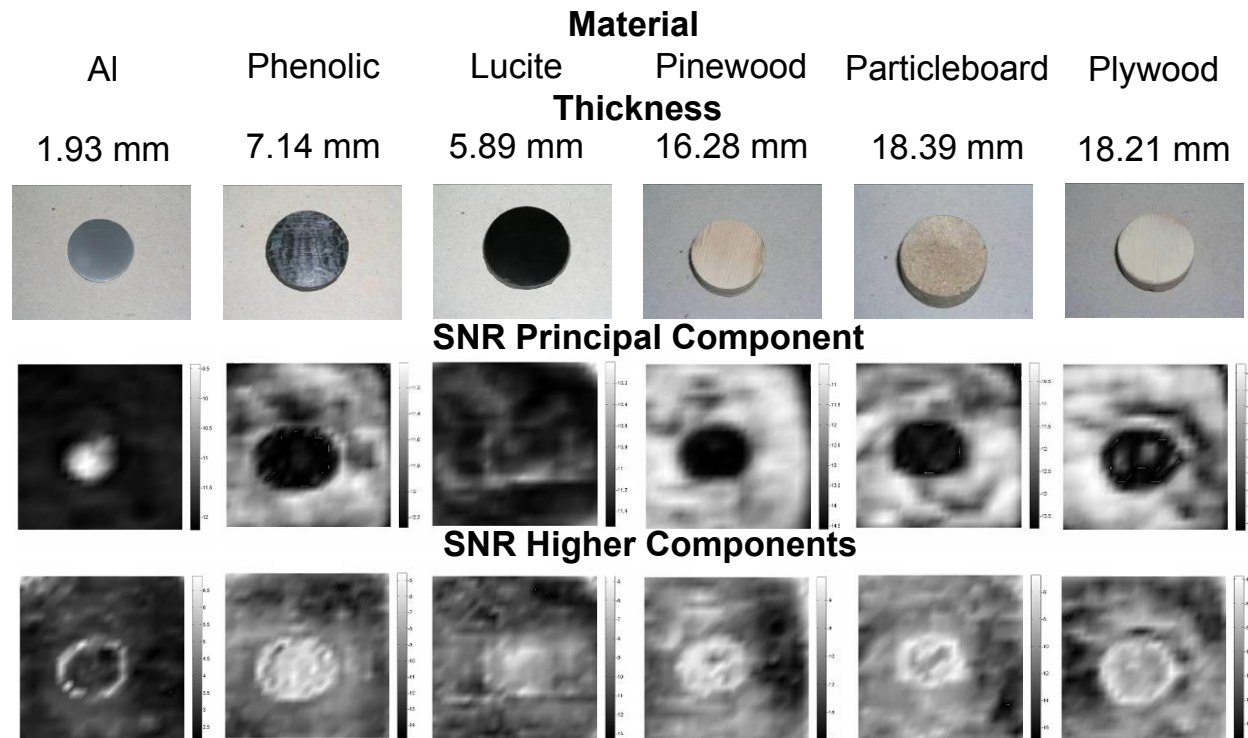


Fig. 10. Images of the SNR of the principal and higher components of 6 pucks 5 cm in diameter of various thickness made of Aluminum, Phenolic, Lucite, Pinewood, Particleboard, and Plywood buried 5 cm beneath soil, at 5 mm step size, and flat soil surface.

5. CONCLUSION

An experimental 90-140 GHz mmW imaging system was developed and tested using different types of objects. The principal application was the detection of landmines and minefield debris buried in soil. The final data set was a collection of mmW images at different frequencies. A signal processing method based on a Principal Component Analysis was applied to the images in order to separate different structures that help to identify the objects. In most cases, the first principal component appeared strongly related to the structure of the object. Information in the higher components was also extracted giving additional information about the composition of the object. The mmW imaging system and PCA method were successful as a means of locating and identifying the non-metallic objects buried beneath the soil. A hyperspectral mmW imaging system using the PCA method is a promising technique for the detection of the landmines and unexploded ordnances.

ACKNOWLEDGMENTS

We would like to thank Mark Cumo of the US Army Night Vision & Electronic Sensors Directorate for providing the landmines used in this study. This work was supported by Northrop Grumman Corporation, Integrated Systems Division, Melbourne, FL.

REFERENCES

1. United Nations Mine Clearance and Policy Unit, Department of Humanitarian Affairs, "Landmines Fact Sheet", <http://www.un.org/Pubs/CyberSchoolBus/banmines/facts.asp>, (Sept 1997).
2. K. Kowalenko, "Saving lives, one land mine at a time," *The Institute* **28**, 10, 2004.

3. M. Acheroy, "Mine action: status of sensor technology for close-in and remote detection of antipersonnel mines," in *Proc. Of 3rd International Workshop on Advanced Ground Penetrating Radar* (Delft, Netherlands, 2005), pp. 3-13.
4. M. Schachne, L. van Kempen, D. Milojevic, H. Sahli, Ph. Van Ham, M. Acheroy, and J. Cornelis, "Mine detection by means of dynamic thermography: simulation and experiments," in *the Second International Conference on the Detection of Abandoned Landmines* (1998), pp. 124-128.
5. L. Yujiri, B. Hauss, and M. Shoucri, "Passive millimeter wave sensors for detection of buried mines," in *Detection Technologies for Mines and Minelike Targets*, A. Dubey, I. Cindrich, J. Ralston, and K. Rigano, eds., Proc. SPIE **2496**, 2-6, (1995).
6. H. Zhong, N. Karpowicz, J. Partridge, X. Xie, J. Xu, and X.-C. Zhang, "Terahertz Wave Imaging for Landmine Detection," in *Terahertz for Military and Security Applications II*, R. J. Hwu and D. L. Woolard, eds., Proc. SPIE **5411**, 33-44, (2004).
7. T. W. Du Bosq, R. E. Peale, A. Weeks, J. Grantham, D. Dillery, D. Lee, D. Muh, and G. D. Boreman, "Terahertz/millimeter wave characterizations of soils for mine detection: transmission and scattering," in *Terahertz for Military and Security Applications III*, R.J. Hwu, D.L. Woolard, and M.J. Rosker, editors, Proc. Of SPIE vol. 5790, 66-73 (2005).
8. X. Miao, M. R. Azimi-Sadjadi, B. Tian, A. C. Dubey, and N. H. Witherspoon, "Detection of mines and minelike targets using principal component and neural-network methods," *IEEE Trans. Neural Networks* **9**, 454-463 (1998).
9. M. R. Azimi-Sadjadi, D. E. Poole, S. Sheedvash, K. D. Sherbondy, and S. A. Stricker, "Detection and classification of buried dielectric anomalies using a separated aperture sensor and a neural network discriminator," *IEEE Trans. Inst. Meas.* **41**, 137-143 (1992).
10. B. Karlsen, J. Larsen, H. B. D. Sorensen, K. B. Jakobsen, "Comparison of PCA and ICA based clutter reduction in GPR systems for anti-personal landmine detection," in *Proceedings of IEEE Conference on Statistical Signal Processing* (2001), pp. 146-149.
11. National Defence Mine/Countermine Information Centre, The Department of National Defence, "Landmine Data Sheet," <http://ndmic-cidnm.forces.gc.ca> (August 2005).
12. D. F. Morrison, *Multivariate Statistical Methods, 3rd ed.* (McGraw-Hill, Singapore, 1990).
13. J.M.Lopez-Alonso, J. Alda, and E. Bernabeu, "Principal components characterization of noise for infrared images," *Appl. Opt.* **41**, 320-331 (2002).
14. J. Kositsky, R. Cosgrove, C. Amazeen, and P. Milanfar, "Results from a forward-looking GPR mine detection system," in *Detection and Remediation Technologies for Mines and Minelike Targets VII*, J. T. Broach, R. S. Harmon, G. J. Dobeck, eds., Proc. SPIE **4742**, 206-217, (2002).
15. W. R. Folks, J.M. Lopez-Alonso, B. Monacelli, A. Weeks, G. Zummo, D. Mullally, G. D. Boreman, "Characterization of digital-micromirror device-based infrared scene projector," *Opt. Eng.* **44**, 086402 (2005).
16. Lopez Alonso, J.M, Monacelli B., Alda J., Boreman G., "Uncertainty analysis in the measurement of the spatial responsivity of infrared antennas", *Appl. Opt.* **44**, 4557-4568 (2205).
17. J. M. López-Alonso, J. M. Rico-García, and J. Alda, "Photonic crystal characterization by FDTD and principal component analysis," *Optics Express* **12**, 2176-2186 (2004).
18. Schumaker, Wood, and Thacker, *Infrared Imaging Systems Analysis* (DCS Corporation, Ann Arbor, MI, 1998).